PROCEEDINGS OF SCIENCE

Measurement of Cross Sections of Electroweak and Total Production of $Z\gamma jj$ at 13 TeV with ATLAS

Gitanjali Poddar[a,*] **on behalf of ATLAS Collaboration**

[a] *Laboratoire d'Annecy De Physique Des Particules (LAPP), 9 Chemin de Bellevue, Annecy, France*

E-mail: gitanjali.poddar@cern.ch

This analysis reports the cross-section measurements of a $Z\gamma$ pair in association with two jets, utilising 140 fb^{-1} of LHC proton–proton collision data collected from 2015–2018. The fiducial cross-section for electroweak production is measured at 3.6±0.5 fb, with a significance exceeding five standard deviations. Including contributions from strong interactions, the total fiducial cross-section is $16.8^{+2.0}_{-1.8}$ fb. All results align with Standard Model predictions. Differential cross-sections are also measured, exhibiting good agreement with Monte Carlo (MC) predictions.

The Eleventh Annual Conference on Large Hadron Collider Physics (LHCP2023)
22-26 May 2023
Belgrade, Serbia

*Speaker

© Copyright owned by the author(s) under the terms of the Creative Commons Attribution-NonCommercial-NoDerivatives 4.0 International License (CC BY-NC-ND 4.0).

PoS(LHCP2023)258

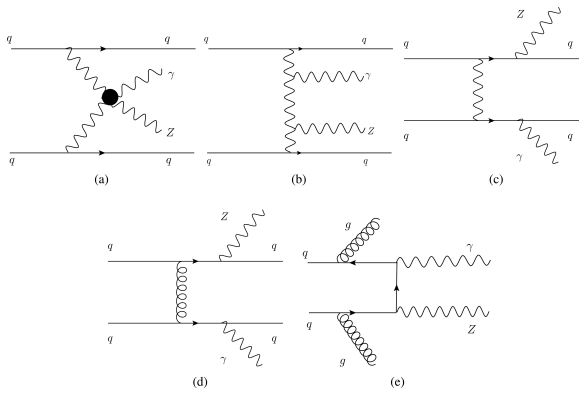

Figure 1: Representative Feynman diagrams of the processes relevant to this analysis: (a) quartic gauge coupling VBS, (b) triple gauge coupling VBS, (c) electroweak non-VBS, QCD-induced process with (d) gluon exchange or (e) gluon radiation. [2]

1. Introduction

Vector boson scattering (VBS) processes are a potent test of the Standard Model (SM) since they can help extract constraints on anomalous quartic gauge couplings (aQGCs)[1]. The examination of $Z\gamma$ VBS is particularly significant as it probes neutral quartic couplings forbidden at lowest order of the SM. At the LHC, $Z\gamma$ VBS involves a final state with a $Z\gamma$ pair and two jets ($Z\gamma jj$). However, there are additional processes that contribute to the same state, as depicted in Figure 1. Notably, $Z\gamma jj$ processes from electroweak mechanisms (i.e. top row of Figure 1) cannot be disentangled due to gauge invariance. Therefore, a comprehensive study of $Z\gamma$ VBS at the LHC entails exploring the entire EW-$Z\gamma jj$ production.

This analysis [2][3] explores EW-$Z\gamma jj$ production using proton-proton collision data recorded by the ATLAS detector [4] from 2015 to 2018. Additionally, it explores total $Z\gamma jj$ production, that includes EW-$Z\gamma jj$, QCD-$Z\gamma jj$, and their interference. This complements the recent ATLAS $Z\gamma$+jets analysis [5] by measuring the total $Z\gamma jj$ process in a VBS-like region and thus enhancing our understanding of the process in a region sensitive to new physics.

2. Event Selection

In this analysis, $Z\gamma jj$ events are chosen with Z decaying leptonically to e^+e^- or $\mu^+\mu^-$ pairs.[1] Leading (sub-leading) leptons must have $p_T^l > 30$ (25) GeV, the photon $p_T^\gamma > 25$ GeV, and jets $p_T^j > 50$ GeV. Additional criteria based on typical VBS topology[6] include i) two *tagging jets* from incoming quarks with wide rapidity separation ($|\Delta y| > 1$) and large invariant mass (m_{jj}>150 GeV), ii) suppression of hadronic activity between tagging jets ($N_{gap}^{jets} = 0$) due to the absence of color flow between incoming quarks, and iii) centrally located pair of vector bosons with respect to tagging jets, measured by $\zeta = |\frac{y_{Z\gamma} - (y_{j1}+y_{j2})/2}{y_{j1}-y_{j2}}| < 0.4$. Furthermore, to reduce final state radiation, m_{ll}+$m_{ll\gamma}$ must be greater than 182 GeV. Additionally, m_{ll} must exceed 40 GeV to remove low mass resonances. Lastly, to mitigate background from $\bar{t}t\gamma$ processes, events with b-jets are vetoed.

[1] $Z \to \tau^+\tau^-$ events are excluded due to their negligible contribution. [3]

PoS(LHCP2023)258

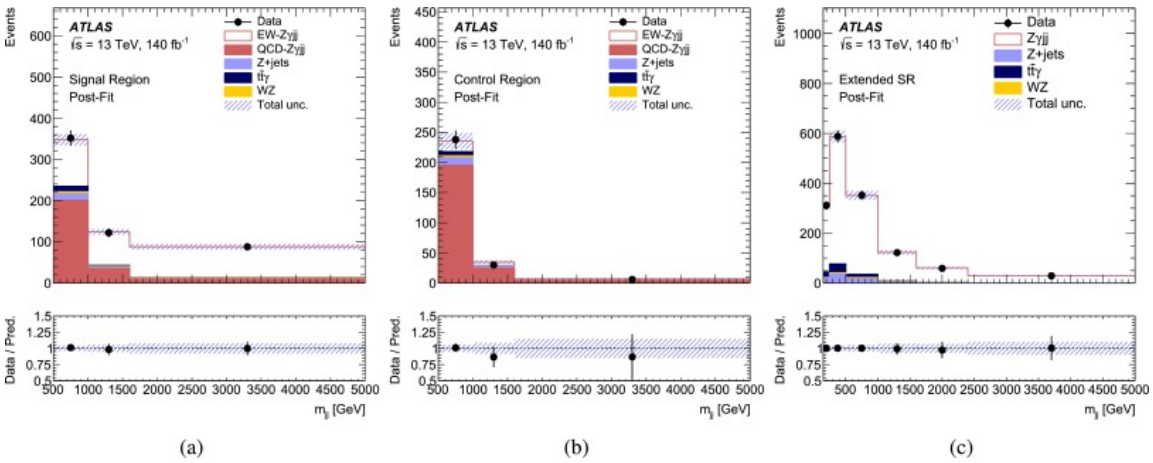

Figure 2: Post-fit mjj distributions in (a) the $m_{jj} > 500$ GeV SR (b) the $m_{jj} > 500$ GeV CR and (c) the $m_{jj} > 150$ GeV Extended SR. The uncertainty band around the expectation includes all systematic uncertainties. The error bar around the data points represents the data statistical uncertainty. All overflow events are included in the last bin.

3. Background Estimation

In the EW-$Z\gamma jj$ analysis, QCD-$Z\gamma jj$ is the main background. It is estimated from MC and validated in a QCD-enriched control region. For both EW and total $Z\gamma jj$ analyses, Z+jets background is estimated using a data-driven two-dimensional sideband method employing photon identification and isolation, $t\bar{t}\gamma$ background is estimated from MC simulation and validated in a $e\mu\gamma$ control region and the minor background from $WZjj$ events is estimated from simulation.

4. Measurement Regions

In the EW-$Z\gamma jj$ analysis, Signal Region (SR) and Control Region (CR) are defined by $\zeta < 0.4$ and $\zeta > 0.4$ respectively. The m_{jj} cut is increased to 500 GeV to ensure accurate extrapolation of QCD-$Z\gamma jj$ process shape from CR to SR [3]. For the total $Z\gamma jj$ analysis, a QCD-enriched CR is unnecessary as QCD-$Z\gamma jj$ is part of the signal. Moreover, the m_{jj} cut is kept at 150 GeV for increased statistics, defining this measurement region as the Extended SR.

5. Analysis Procedure

To measure the EW-$Z\gamma jj$ fiducial cross-section, a simultaneous profile-likelihood fit to the m_{jj} distribution is conducted in SR and CR using `TRExFitter`[7]. The parameter of interest (POI) is $\mu_{EW} = \sigma^{EW}_{\text{data}}/\sigma^{EW}_{\text{MC}}$. The fit also constrains the normalisation of the QCD-$Z\gamma jj$ background. The cross-section is then obtained by multiplying μ_{EW} with the expected cross-section at the particle level. For the $Z\gamma jj$ cross-section, a similar fit is performed in the Extended SR, with $\mu_{Z\gamma}$ as the POI and no normalisation constraint for QCD-$Z\gamma jj$. Post-fit distributions are shown in Figure 2.

To measure EW-$Z\gamma jj$ and $Z\gamma jj$ differential cross-sections in the fiducial phase space, data distributions are unfolded (i.e. corrected for background and detector effects) via the profile-likelihood

PoS(LHCP2023)258

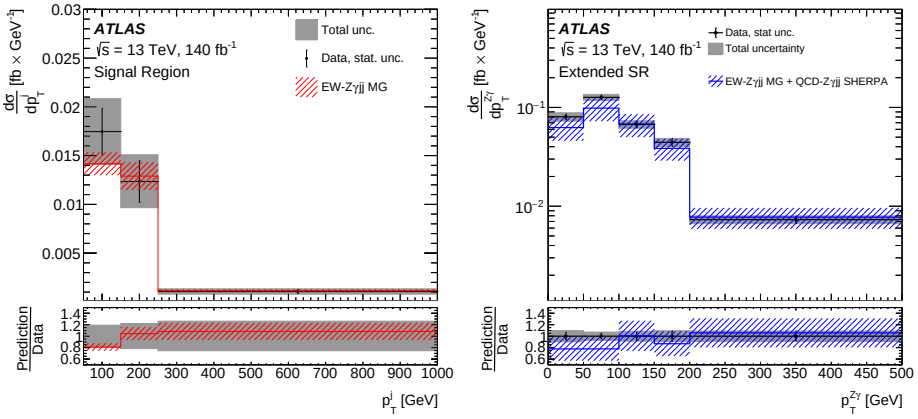

Figure 3: Differential measurements of EW-$Z\gamma jj$ as a function of p_T^j (left) and total $Z\gamma jj$ as a function of $p_T^{Z\gamma}$ (right). The lower panels show the ratios of the MC predictions to the data. The band around the unfolded data represents the total uncertainty. The hatched area represents the uncertainty in the prediction. All overflow events are included in the last bin.

unfolding (PLU) method in `TRExFitter`. In short, PLU treats unfolding as a profile-likelihood fit, by applying normalisation factors to each particle-level bin of the measured observable. Additionally, in the EW-$Z\gamma jj$ analysis, the normalisation of QCD-$Z\gamma jj$ background is constrained per bin simultaneously during the unfolding process.

6. Results

The measured EW-$Z\gamma jj$ cross-section is 3.6±0.5 fb, consistent with the `MADGRAPH5_aMC@NLO 2.6.5`[8] SM prediction of 3.5±0.2 fb. The measured $Z\gamma jj$ cross-section is $16.8^{+2.0}_{-1.8}$ fb, in agreement with `MADGRAPH5_aMC@NLO 2.6.5` and `SHERPA 2.2.11`[9][10] SM prediction of $15.7^{+5.0}_{-2.6}$ fb. The primary uncertainty arises from EW-$Z\gamma jj$ and QCD-$Z\gamma jj$ modelling respectively.

Differential cross-section measurements cover various variables for distinct physics motivations: i) m_{jj}, $|\Delta y|$, p_T^l, p_T^j for modelling studies, and ii) $p_T^{Z\gamma}$, E_T^γ, $\Delta\phi(Z\gamma, jj)$ for Effective Field Theory (EFT) studies. Additional measurements for modelling studies include p_T^Z and ζ in the context of the $Z\gamma jj$ process. Two of these results are shown in Figure 3. All findings are consistent with SM expectations, with data statistics being the primary source of uncertainty.

7. Conclusion

The primary outcome of this analysis is the first observation of EW-$Z\gamma jj$ with the ATLAS detector. It also presents the first set of EW-$Z\gamma jj$ differential measurements with the ATLAS detector. Notably, EW-$Z\gamma jj$ differential measurements of $p_T^{Z\gamma}$ and $\Delta\phi(Z\gamma, jj)$ are performed for the first time at the LHC. The analysis also presents cross-section measurements of the total $Z\gamma jj$ process. Notably, $Z\gamma jj$ differential measurements of p_T^Z and ζ are performed for the first time at the LHC too. These outcomes will significantly contribute to future studies, especially in the exploration of aQGCs and in assisting MC modelling studies.

PoS(LHCP2023)258

References

[1] O. J. P. Éboli, M. C. Gonzalez-Garcia, and J. K. Mizukoshi, *$pp \to jje^{\pm}\mu^{\pm}\nu\nu$ and $jje^{\pm}\mu^{\mp}\nu\nu$ at $O(\alpha_{em}^6)$ and $O(\alpha_{em}^4\alpha_s^2)$ for the study of the quartic electroweak gauge boson vertex at CERN LHC*, Phys. Rev. D **74** 073005, 2006

[2] G. Aad et al., *Measurement of the cross-sections of the electroweak and total production of a $Z\gamma$ pair in association with two jets in pp collisions at $\sqrt{s} = 13$ TeV with the ATLAS detector*, Phys. Lett. B **846** 138222, 2023

[3] G. Poddar, *Study of $Z\gamma$ Vector Boson Scattering and Upgrade of Liquid Argon Electronic Calibration Board with ATLAS detector*, https://cds.cern.ch/record/2884912?ln=en

[4] ATLAS Collaboration, *The ATLAS Experiment at the CERN Large Hadron Collider*, JINST **3** S08003, 2008

[5] G. Aad et al., *Measurements of $Z\gamma$+jets differential cross sections in pp collisions at $\sqrt{s} =$ 13 TeV with the ATLAS detector*, JHEP **07** 072, 2023

[6] D. L. Rainwater, R. Szalapski and D. Zeppenfeld, *Probing color singlet exchange in Z + two jet events at the CERN LHC*, Phys. Rev. D **54** 6680, 1996

[7] TRExFitter, https://trexfitter-docs.web.cern.ch/trexfitter-docs/

[8] J. Alwall et al., *The automated computation of tree-level and next-to-leading order differential cross sections, and their matching to parton shower simulation*, JHEP **07** 079, 2014

[9] *Sherpa Manual Version 2.2.11*, https://sherpa.hepforge.org/doc/SHERPA-MC-2.2.11.html

[10] E. Bothmann et al., *Event generation with Sherpa 2.2*, SciPost Physics **7**, 2019

PoS(LHCP2023)258